

A Patch-Based Tensor Decomposition Algorithm for M-FISH Image Classification

Min Wang,^{1,2} Ting-Zhu Huang,¹ Jingyao Li,² Yu-Ping Wang^{2*}

¹School of Mathematical Sciences/
Research Center for Image and Vision
Computing, University of Electronic
Science and Technology of China,
Chengdu, Sichuan 611731, China

²Department of Biomedical Engineering,
Tulane University, New Orleans,
Louisiana 70118

Received 30 September 2015; Revised 25
January 2016; Accepted 1 April 2016

Grant sponsor: 973 Program, Grant num-
ber: 2013CB329404

Grant sponsor: NSFC, Grant number:
61370147

Grant sponsor: Fundamental Research
Funds for the Central Universities, Grant
number: ZYGX2013Z005

Grant sponsor: NIH, Grant number: R01
MH104680, R01 MH107354, R01 GM109068

Additional Supporting Information may be
found in the online version of this article.

*Correspondence to: Yu-Ping Wang,
Department of Biomedical Engineering,
Tulane University, New Orleans, Louisi-
ana 70118.

E-mail: wyp@tulane.edu

Published online 00 Month 2016 in Wiley
Online Library (wileyonlinelibrary.com)

DOI: 10.1002/cyto.a.22864

© 2016 International Society for
Advancement of Cytometry

• Abstract

Multiplex-fluorescence in situ hybridization (M-FISH) is a chromosome imaging technique which can be used to detect chromosomal abnormalities such as translocations, deletions, duplications, and inversions. Chromosome classification from M-FISH imaging data is a key step to implement the technique. In the classified M-FISH image, each pixel in a chromosome is labeled with a class index and drawn with a pseudo-color so that geneticists can easily conduct diagnosis, for example, identifying chromosomal translocations by examining color changes between chromosomes. However, the information of pixels in a neighborhood is often overlooked by existing approaches. In this work, we assume that the pixels in a patch belong to the same class and use the patch to represent the center pixel's class information, by which we can use the correlations of neighboring pixels and the structural information across different spectral channels for the classification. On the basis of assumption, we propose a patch-based classification algorithm by using higher order singular value decomposition (HOSVD). The developed method has been tested on a comprehensive M-FISH database that we established, demonstrating improved performance. When compared with other pixel-wise M-FISH image classifiers such as fuzzy c-means clustering (FCM), adaptive fuzzy c-means clustering (AFCM), improved adaptive fuzzy c-means clustering (IAFCM), and sparse representation classification (SparseRC) methods, the proposed method gave the highest correct classification ratio (CCR), which can translate into improved diagnosis of genetic diseases and cancers. © 2016 International Society for Advancement of Cytometry

• Key terms

M-FISH; tensor decomposition; HOSVD; chromosome image classification; image segmentation; cytogenetics

CHROMOSOME is the carrier of genetic information. A normal human has 46 chromosomes, which are arranged into 22 pairs of similar, homologous autosomes and two sex determinative chromosomes (XY-male, XX-female). Karyotyping is the process by which geneticists take images of the chromosomes when the cell is undergoing mitosis and classify the chromosomes into 23 or 24 classes based on their banding patterns. Since this process is both time consuming, expensive and difficult to automate for detecting chromosome aberrations, a combinatorial labeling technique called multiplex-fluorescence in situ hybridization (M-FISH) (1,2) has been developed to achieve a higher sensitivity, specificity, and resolution than is possible by banding analysis (karyotyping). This technology uses five color dyes that attach to specific sequences of DNA in ways that each chromosome class is labeled with a unique combination of dyes and another DNA dye known as 4-6-diamidino-2-phenylindole (DAPI) is used to stain all chromosomes. A fluorescent microscope with multiple optical filters is used to capture the chromosome images, where each dye is visible in a particular wavelength. Using combinatorial labeling, M-FISH images can be obtained as multispectral or multichannel images, in which each pixel at each channel is either visible (signed as "1") or not (signed as "0"). Figure 1 shows

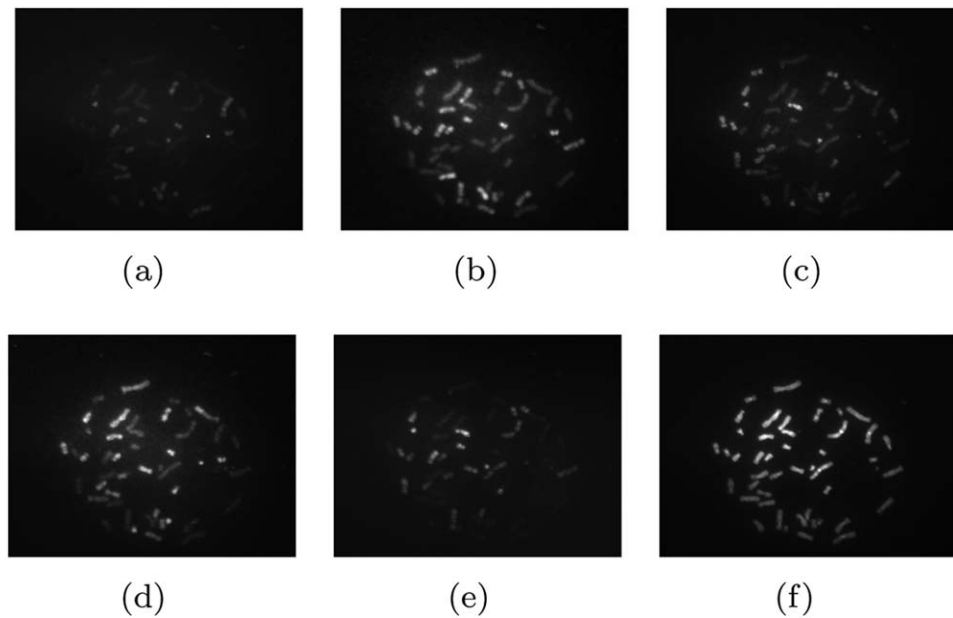


Figure 1. An example of the M-FISH image set. (a) S Aqua A-channel. (b) S Gold F-channel. (c) S Green G-channel. (d) Red R-channel. (e) S Red Y-channel. (f) DAPI D-channel.

an example of M-FISH image set, which is collected by a fluorescent microscope with multiple optical filters. S Aqua (A), S Gold (F), S Green (G), Red (R), S Red (Y), DAPI (D) are six dyes that are used to paint the chromosomes. Only some parts of chromosomes are visible in the first 5 channels, but all of the chromosomes can be observed in the DAPI channel. The number of boolean combinations for n is $2^n - 1$. Hence, there are 31 combinations for 5 fluors, which are sufficient to distinguish the 24 classes of chromosomes in human genome. These six images form multichannel representations of chromosomes, by which pixel-wise classification of human chromosome is possible.

M-FISH is used for detecting chromosome abnormalities. For example, chromosomal translocation (3) is the exchange of chromosome materials within the same or between different chromosomes. M-FISH imaging can be used to quickly

visualize or detect this type of chromosome abnormality, since pixels in the region of translocation can be displayed in different pseudo-colors after image classification, that is, color karyotyping. Even though M-FISH imaging greatly simplifies the process of karyotyping, visual inspection is still a laborious process, especially for small rearrangements of chromosome materials. Many attempts have been made to automate the process of M-FISH image analysis (4–9), but the reliability of the technique has not yet reached the level for clinical application (8–11). To improve the accuracy of chromosomal aberrations detection, accurate classification algorithms are always desirable. The algorithms for classification of M-FISH images can be divided into two categories: pixel-by-pixel classification (5,7,12–15) and region-based classification (8,16–19). The pixel-by-pixel classification approaches either first segment the chromosome pixels from the background using DAPI

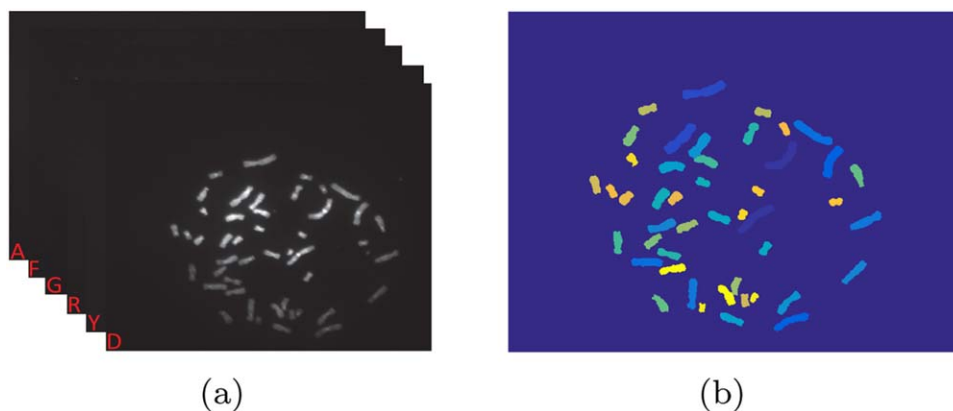


Figure 2. (a) A multichannel M-FISH image. (b) Ground truth of classification. [Color figure can be viewed in the online issue, which is available at wileyonlinelibrary.com.]

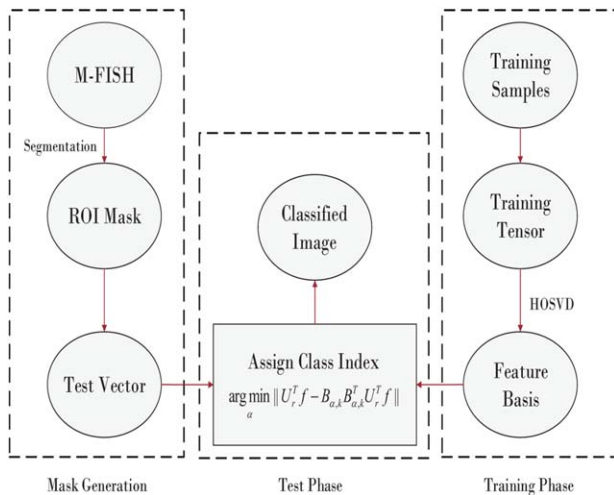


Figure 3. Flowchart of the proposed method. [Color figure can be viewed in the online issue, which is available at wileyonlinelibrary.com.]

channel and then perform classification (6,8,11,12,15,18,20) or directly classify the background pixels as a new class (4,5,7,21). Even with preprocessing and postprocessing, the classification accuracy is still not high enough for clinical use (less than 90%) (4,7,9,15,19). Figure 2 shows a multichannel M-FISH image and its ground truth. The classification result is displayed by using 24 pseudo-colors. For a normal cell, each class of chromosomes should be painted with the same color. From Figure 2b, we can see that the number of background pixels is much larger than the number of chromosome pixels. In Figure 2b, we can also see that the neighbor pixels belong to the same class with a high probability. In this work, we employ the pixels in a patch to take into account of this neighborhood information. The size of a pixel value vector is $5s^2$, because the number of channel images is 5 and the patch size is $s \times s$. In this way, we utilize the correlations of neighboring pixels as well as structural information across five spectral channels for the classification. On the basis of high dimensional feature vector space, we can effectively classify the chromosome pixels into 24 classes. In addition, the classification is performed in the chromosome region, which is generated by segmenting the chromosome pixels from background from DAPI channel image.

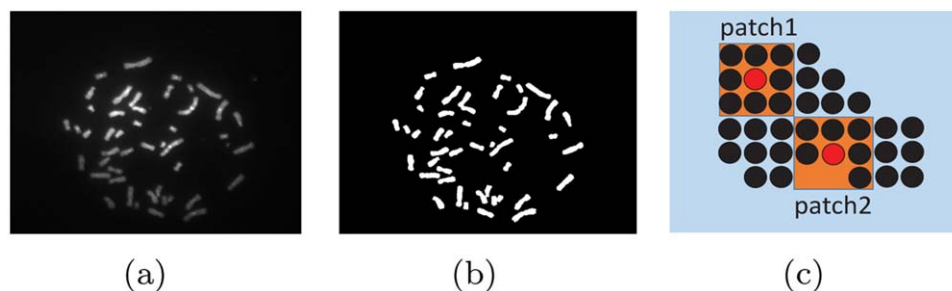


Figure 4. An example of ROI mask and the patches used. (a) DAPI channel. (b) ROI mask. (c) Patches in a mask. [Color figure can be viewed in the online issue, which is available at wileyonlinelibrary.com.]

Chromosome classification has been well studied with various approaches and in this article we exploit the use of tensor decomposition methods, which have recently attracted great interests in signal processing, data analysis, and machine learning (22–29). Among them, higher order singular value decomposition (HOSVD) (30) is a special example of tensor decompositions, which is widely used in classification, feature extraction, and subspace-based harmonic retrieval (31–35). Approaches to two-way component analysis including principal component analysis (PCA), independent component analysis (ICA), nonnegative matrix factorization (NMF), and sparse component analysis (SCA) (36–40) have been well established. Early multiway data analysis methods first reformat the data tensor as a matrix, and then process it with two-way approaches. However, such a flattened view and the reshaping of the data will destroy inherent multidimensional structure in the data, where hidden components within multiway data cannot be discovered. To this end, we construct a three-way training tensor to learn the intrinsic features from multi-channel imaging data. The basic tensor concepts used in our work can be found in Supporting Information Appendix A. We will perform HOSVD on the training tensor to extract the features of each chromosome class simultaneously. After HOSVD, we can reduce the dimension of feature representations or obtain a low-dimensional feature space. Finally, we project an unknown pixel vector into the low dimensional feature space and assign it to the class, where it can be best represented by the low dimensional features corresponding to that particular class. Both training samples and unknown pixel vectors are obtained by vectorizing pixels from a cross-channel patch size of $s \times s \times 5$.

The contributions of our work are twofold. First, we use the patch to represent a central pixel within a small region so that we can fully utilize the correlations of neighboring pixels and structural information across multiple spectral channels. Second, we employ HOSVD to extract the features for each chromosome class, obtaining a low dimensional feature representation. Finally, an unknown pixel is projected into the same feature space and is assigned the class label to which it has the closest distance. As a result, we have a novel patch-based tensor decomposition algorithm for M-FISH images classification. This is similar to PCA by projecting the data into a low dimensional space that can best represent each class

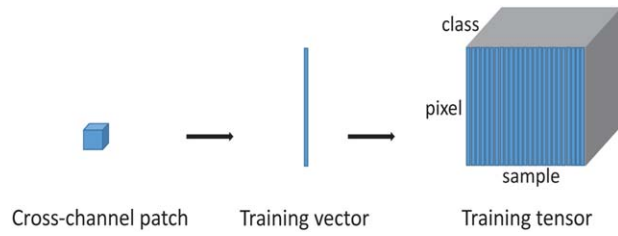


Figure 5. The process of constructing the training tensor. [Color figure can be viewed in the online issue, which is available at wileyonlinelibrary.com.]

of chromosome. The chromosome region is generated by segmenting DAPI channel image, where all chromosomes are visible. The remainder of the article is organized as follows. In Algorithm Section, we describe the details of the proposed algorithm. In Experimental Results Section, we evaluate the algorithm by testing on a comprehensive M-FISH image database (Available: <http://sites.google.com/site/xiaobaocao006/database-for-download>) established by us. The article is concluded with a summary and discussion.

ALGORITHM

In this section, we will present the details of the proposed algorithm. Figure 3 shows the flowchart of the proposed method. There are seven steps in the procedure, which can be divided into three phases. The first phase is to generate the mask of region of interest (ROI), only within which the pixels are classified. This is also called chromosome segmentation. The second is the training phase in which we construct the training tensor, which will be used by HOSVD to extract features for each type of chromosome. The third is the test phase in which we determine the class label of an unknown testing pixel.

Mask Generation-Segmentation

Since only chromosomal region is of interest and it is very time consuming to classify all the pixels if we consider the background pixels as a new class. So we focus on chromosomal region. A level set-based image segmentation method (41) is used to segment DAPI channel image to generate the mask of ROI, containing all chromosome pixels. Only pixels within this mask are classified using the proposed classification algorithm. Since neighboring pixels within a small region and across multiple channels share the similar features and therefore may belong to the same class, we use the cross-channel patch with the size of $s \times s \times 5$ to represent the information of a central pixel. Let $\mathcal{X} \in \mathbb{R}^{m \times n \times 5}$ denote the tensor, which consists of five channels of M-FISH images (e.g., A, F, G, R, Y channels) and a DAPI channel image. $D \in \mathbb{R}^{m \times n}$ denote the DAPI channel image, where $m \times n$ is the image size. After the segmentation of the DAPI channel image, we get the ROI mask denoted by $M \in \mathbb{R}^{m \times n}$. $M(i, j) = 0$ if $D(i, j)$ is a background pixel; otherwise $M(i, j) = 1$. Figure 4 shows an example of ROI mask and its patches. Figure 4a is the original DAPI channel image, where all chromosomes in the image are

visible. Figure 4b is the ROI mask obtained from the segmentation of Figure 4a. Figure 4c shows the patches with the size of 3×3 in a mask. Each patch contains the centre pixel colored with red. As we can see from Figure 4c, patch1 consists of chromosome pixels without background while patch2 contains background pixels. These two patches contain two types of pixels in the ROI mask: patch1 contains inside pixels while patch2 has boundary pixels. For both cases, the information of the center pixel can be well represented by the patch.

Training Phase

The training samples we used are cross-channel patches, which are extracted from $\mathcal{X} \in \mathbb{R}^{m \times n \times 5}$ randomly. Figure 5 shows the process of how to construct the training tensor. A cross-channel patch in $\mathbb{R}^{s \times s \times 5}$ are reshaped into a vector in \mathbb{R}^{5s^2} . All of them are arranged into different matrices to construct the training tensor so that every frontal slice contains the vectorized cross-channel patches for one chromosome class. The training tensor has three modes: mode-1 for pixel, mode-2 for sample and mode-3 for class. We denote it by $\mathcal{F} \in \mathbb{R}^{5s^2 \times p \times q}$, where $5s^2$ is the dimension of pixel-mode, that is, the dimension of training vector; p is the dimension of sample-mode, that is, the number of training vectors used in each chromosome class; q is the dimension of class-mode, that is, the number of all chromosome classes (e.g., $q = 23$ for the female cell and $q = 24$ for the male cell). HOSVD is a powerful tensor decomposition method to extract the features of each mode simultaneously, as described in Supporting Information Appendix. Let \mathcal{F} have the HOSVD

$$\mathcal{F} = \mathcal{G} \times_1 U \times_2 V \times_3 W \approx \mathcal{D} \times_1 U_r \times_2 V, \quad (1)$$

where $\mathcal{G} \in \mathbb{R}^{5s^2 \times p \times q}$, $U \in \mathbb{R}^{5s^2 \times 5s^2}$, $V \in \mathbb{R}^{p \times p}$, $W \in \mathbb{R}^{q \times q}$, $U_r = U(:, 1:r)$, and $\mathcal{D} = \mathcal{G}(1:r, :, :) \times_3 W \in \mathbb{R}^{r \times p \times q}$. Figure 6 illustrates the process of HOSVD described in Eq. (1). The standard orthogonal column vectors in U , V , and W are the feature vectors of pixel-mode, sample-mode and class-mode, respectively. HOSVD gives U , V , and W by using the information from the training tensor, which constitute the basis matrices of all the chromosome classes in pixel-mode, sample-mode and class-mode, respectively. Since the dimension of pixel-mode increases along with the increase of s , we take the r leading feature vectors of U to form a subspace to compactly represent the pixel mode. By this approximation, we reduce the representation of the pixel from \mathbb{R}^{5s^2} to \mathbb{R}^r . According to the orthogonality of U_r and V , \mathcal{D} can be obtained by [Eq. (2)]

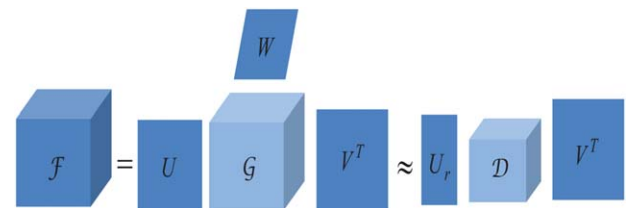


Figure 6. The HOSVD of training tensor. [Color figure can be viewed in the online issue, which is available at wileyonlinelibrary.com.]

Algorithm 1. M-FISH image classification by HOSVD

Input: Five M-FISH images $\mathcal{X} \in \mathbb{R}^{m \times n \times 5}$ and the DAPI channel image $D \in \mathbb{R}^{m \times n}$.

Mask generation:

<1> Segment the DAPI channel to get the ROI mask $M \in \mathbb{R}^{m \times n}$.

Training phase:

<2> Construct the training tensor $\mathcal{F} \in \mathbb{R}^{5s^2 \times p \times q}$ by following Figure 5.

<3> Compute the parameter r and k by 10-fold cross validation.

<4> Compute the HOSVD of the training tensor \mathcal{F} by Eq. (1).

<5> Compute and store the feature vectors of each chromosome class into $B_{\alpha,k} \in \mathbb{R}^{r \times k}$ by Eqs. (2) and (3).

Test phase:

<6> For each unclassified pixel in ROI mask, extract the cross-channel patch in $\mathbb{R}^{s \times s \times 5}$ and reshape it into a test vector $f \in \mathbb{R}^{5s^2}$.

<7> Compute the residual for each chromosome class by Eq. (6) and assign the class index giving smallest residual to the pixel.

Output: The classified image that chromosome pixels were assigned to class index.

$$D = \mathcal{F} \times_1 U_r^T \times_2 V^T \in \mathbb{R}^{r \times p \times q}. \quad (2)$$

In particular, $D_\alpha = D(:, :, \alpha) \in \mathbb{R}^{r \times p}$ is the α th frontal slice of tensor D , which consists of the basis vectors for the α th

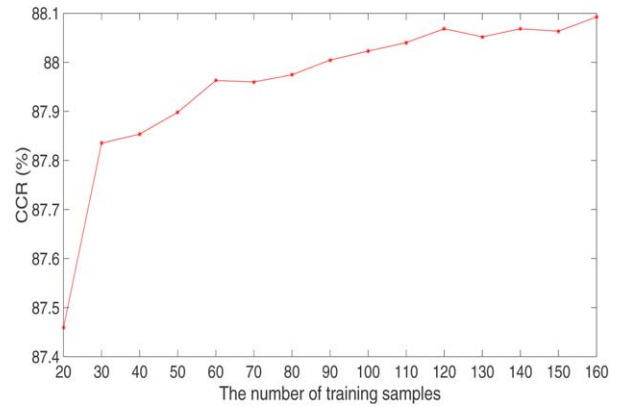


Figure 8. The CCRs with different number of training samples. [Color figure can be viewed in the online issue, which is available at wileyonlinelibrary.com.]

chromosome class. To get the orthonormal and ordered basis vectors of D_α , we compute the SVD as

$$D_\alpha = B_\alpha \Sigma_\alpha Q_\alpha^T, \quad \alpha = 1, 2, \dots, q. \quad (3)$$

We take the k leading left singular vectors of B_α to form the new basis matrix as $B_{\alpha,k} = B_\alpha(:, 1:k) \in \mathbb{R}^{r \times k}$. It is clear that the columns of $B_{\alpha,k}$ span the dominant subspace of D_α .

Test Phase

In the test phase, every pixel in the ROI mask will be classified by using the feature vectors obtained from training phase. Since our method is patch based, the unclassified pixel located at (i, j) is spanned to form a cross-channel patch in $\mathbb{R}^{s \times s \times 5}$ and then reshaped into a vector $f \in \mathbb{R}^{5s^2}$. We compute

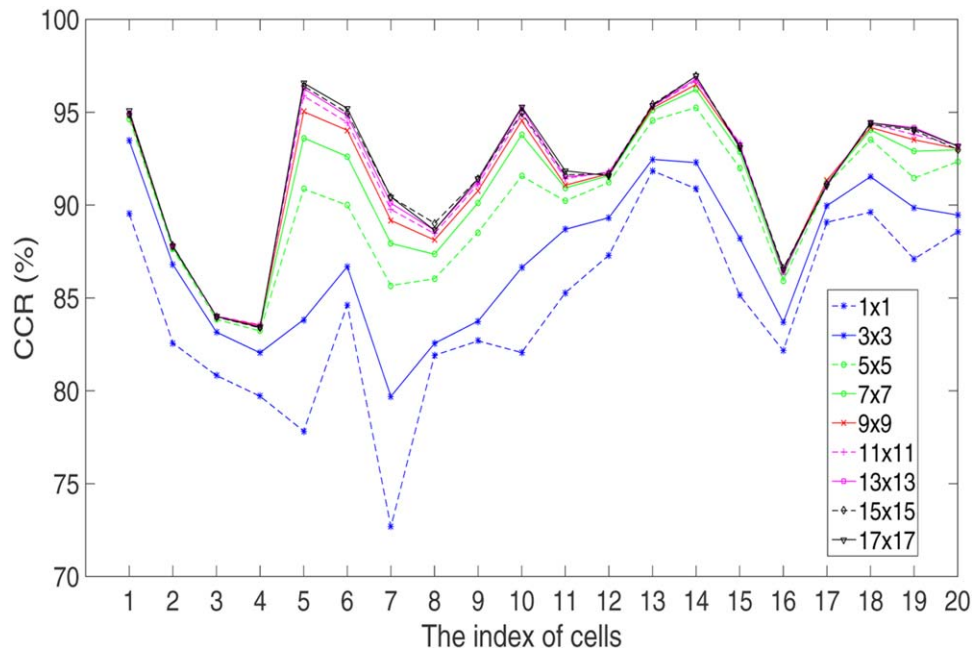


Figure 7. The CCRs with different patch sizes. [Color figure can be viewed in the online issue, which is available at wileyonlinelibrary.com.]

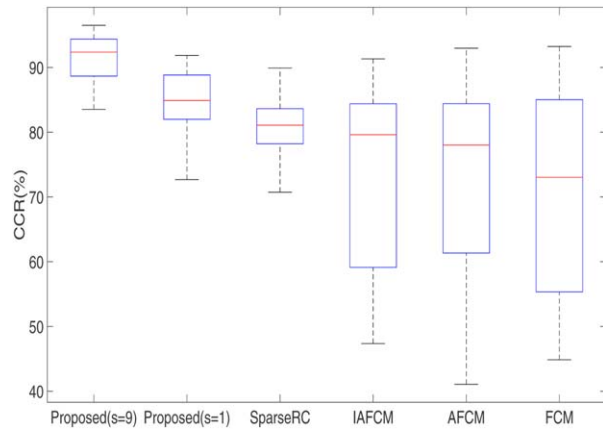


Figure 9. The box plots of M-FISH image classification accuracy using different methods. [Color figure can be viewed in the online issue, which is available at wileyonlinelibrary.com.]

the low dimensional representation $f^* = U_r^T f$ and solve the following least squares problem,

$$\min_{y_\alpha} (f^* - B_{\alpha,k} y_\alpha), \quad \text{for fixed class index } \alpha. \quad (4)$$

Since the columns of $B_{\alpha,k}$ are orthonormal, the solution is given by

$$y_\alpha^* = B_{\alpha,k}^T f^*. \quad (5)$$

Substituting Eq. (5) and $f^* = U_r^T f$ into Eq. (4), we get the class index as

$$\arg \min_{\alpha} \|U_r^T f - B_{\alpha,k} B_{\alpha,k}^T U_r^T f\|, \quad (6)$$

where the index α gives the smallest residual, which is taken to be the predicted class of the unknown pixel. From this process, we can see that we assign the unknown pixel to the class, where it can be best represented with low dimensional feature vector through tensor decomposition.

A direct implementation of the proposed method is presented in Algorithm 1. The key operation HOSVD in <4> requires two SVD computations and two tensor-matrix products, which can be implemented easily by using MATLAB Tensor Toolbox 2.6 (<http://www.sandia.gov/~tgkolda/Tensor-Toolbox/>).

EXPERIMENTAL RESULTS

To test our algorithm, 20 cells (10 males, 10 females) were chosen from the M-FISH database that we have established (Available: <http://sites.google.com/site/xiaobaocao006/database-for-download>). Each M-FISH consists of 6 different channels as in Figure 1. In addition, an annotated image is provided for each M-FISH image set, which is given by experienced cytogeneticists. This image is used as the ground truth, where the gray level of each pixel represents the corresponding chromosome class index. Moreover, background pixels are labeled as 0, and the pixels in the region of overlap are labeled as 255. In our experiments, this classification map serves as the ground truth to evaluate the accuracy of proposed classification method. The correct classification ratio (CCR) is defined by

$$\text{CCR} = \frac{\# \text{chromosome pixels correctly classified}}{\# \text{total chromosome pixels in the image}}. \quad (7)$$

Parameter Determination

There are four parameters in our method that can affect the accuracy of the classification results. They are the patch size s , the number of training samples p , and the number of leading basis vectors r, k . In addition, another parameter is the number of chromosome classes q , which is determined by the test cell ($q = 23$ for the female cell and $q = 24$ for the male cell). Since the patch size s is independent of the number of training samples p , we set $p = 30$ and vary $s \in \{1, 3, 5, 7, 9, 11, 13, 15, 17\}$. The parameter r and k are set by a 10-fold cross validation. Figure 7 shows how the CCR changes with different patch size. It is clear that there is only one pixel in the patch when the patch size is 1×1 . When we enlarge the patch size to $3 \times 3, 5 \times 5, 7 \times 7, 9 \times 9$, CCRs in most of the test cells increase. When the patch size is larger than 9×9 , the correlation of pixels within this larger patch may get lost and the change of CCR is relatively small. This trend of changes verifies that when we use a patch to represent the centre pixel, we can take advantage of the correlations of

Table 1. The mean and STD of CCRs(%) with different classification methods

CELL INDEX	METHODS					
	PROPOSED		SparseRC	IAFCM	AFM	FCM
	S = 9	S = 1				
1	94.87	89.54	89.90	56.91	53.34	58.35
2	87.79	82.57	82.78	58.26	41.88	55.46
3	84.00	80.82	80.01	47.36	41.07	44.86
4	83.52	79.71	77.90	52.16	48.34	53.48
5	95.03	77.83	71.83	59.98	64.66	64.31
6	94.03	84.63	81.31	86.50	78.43	77.58
7	89.18	72.68	70.73	73.09	75.67	45.95
8	88.12	81.91	77.61	79.85	77.58	54.14
9	90.78	82.69	78.52	83.15	81.40	71.96
10	94.54	82.06	75.49	82.40	84.28	77.50
11	91.07	85.28	83.77	48.88	58.02	55.24
12	91.69	87.31	83.47	81.87	85.78	85.55
13	95.23	91.85	89.18	88.93	91.65	93.22
14	96.50	90.88	85.46	91.31	92.97	88.97
15	93.19	85.14	82.54	79.36	84.53	73.66
16	86.49	82.16	80.28	70.03	79.94	72.39
17	91.34	89.08	80.12	76.08	76.77	87.34
18	94.18	89.62	85.67	89.69	91.01	84.85
19	93.52	87.10	80.85	85.62	81.08	85.20
20	93.04	88.56	81.56	82.92	72.14	78.61
mean	91.41	84.57	80.95	73.72	73.03	70.43
std	3.78	4.84	4.90	14.50	16.27	15.27

Table 2. The CCRs (%) of the proposed method with different patch sizes

CELL INDEX	PATCH SIZE (S)								
	1	3	5	7	9	11	13	15	17
1	89.54	93.47	94.64	94.83	94.87	94.96	94.96	94.89	95.07
2	82.57	86.80	87.64	87.71	87.79	87.80	87.77	87.82	87.79
3	80.82	83.16	83.84	84.02	84.00	84.03	84.00	83.98	84.00
4	79.71	82.05	83.23	83.42	83.52	83.56	83.45	83.39	83.42
5	77.83	83.83	90.87	93.62	95.03	95.87	96.29	96.41	96.57
6	84.63	86.69	90.00	92.62	94.03	94.46	94.82	94.96	95.21
7	72.68	79.70	85.67	87.94	89.18	89.77	90.11	90.44	90.44
8	81.91	82.55	86.04	87.36	88.12	88.46	88.65	89.03	88.65
9	82.69	83.76	88.53	90.13	90.78	91.13	91.28	91.43	91.42
10	82.06	86.63	91.57	93.78	94.54	94.88	95.22	94.96	95.29
11	85.28	88.70	90.22	90.93	91.07	91.43	91.52	91.63	91.85
12	87.31	89.32	91.23	91.59	91.69	91.79	91.73	91.70	91.58
13	91.85	92.47	94.56	95.12	95.23	95.32	95.36	95.42	95.36
14	90.88	92.29	95.26	96.22	96.50	96.71	96.80	96.95	96.95
15	85.14	88.23	92.01	92.86	93.19	93.34	93.25	93.17	93.10
16	82.16	83.68	85.90	86.28	86.49	86.48	86.38	86.61	86.54
17	89.08	89.97	91.10	91.23	91.34	91.16	91.12	91.11	91.04
18	89.62	91.53	93.54	94.04	94.18	94.37	94.43	94.36	94.44
19	87.10	89.87	91.46	92.90	93.52	93.80	94.19	94.03	94.10
20	88.56	89.47	92.33	92.98	93.04	93.22	93.18	93.00	93.19
mean	84.57	87.21	89.98	90.98	91.41	91.63	91.73	91.76	91.80
std	4.84	3.95	3.58	3.70	3.78	3.86	3.94	4.91	3.97

neighboring pixels and the structural information across different spectral channels, by which the noise can be suppressed. Since the length of training vector is $5s^2$, a larger patch size will lead to a larger training vector, which will increase the computational load and storage memory. A recommended moderate patch size is 9×9 based on our experiments. We also study the effect of the number of training samples on the CCR, as shown in Figure 8. The comparison was performed in a test cell. We set the patch size as 9×9 and vary the number

of training samples $p \in \{20, 30, 40, 50, 60, 70, 80, 90, 100, 110, 120, 130, 140, 150, 160\}$. From Figure 8, we can see that the CCR gets bigger when p increases. Since the change is less than 0.3% when p increases from 30 to 160, we can know that $p = 30$ is sufficient for the training phase and $p = 30$ is therefore recommended.

The Comparison with Different Methods

The results were also compared with four other existing pixel-wise classification methods: sparse representation classification (SparseRC) (42), improved adaptive fuzzy c-means clustering (IAFCM) (43), adaptive fuzzy c-means clustering (AFCM) (44), and fuzzy c-means clustering (FCM) (12,13) methods that we proposed before. Since we are testing the performance of the classifiers, the classification methods under comparison were processed for the same ROI mask. Table 1 gives results of using different methods for the testing cells. Both the mean value and standard deviations (std) of CCRs are provided. We display the CCRs of the proposed method with patch size $s = 1$ and $s = 9$ in Table 1. When $s = 1$, the proposed method will be degraded to pixel-by-pixel classification, just as the SparseRC, IAFCM, AFCM, and FCM methods, which did not use the correlations of neighboring pixels. From Table 1, we can see that the proposed method with $s = 1$ gives higher mean value of CCRs with smaller standard deviations than SparseRC, IAFCM, AFCM, and FCM methods. This shows that the HOSVD method has more robustness and better performance. As we introduced before, when $s > 1$, the proposed method will use the correlations of neighboring pixels, by which the influence of noise will be

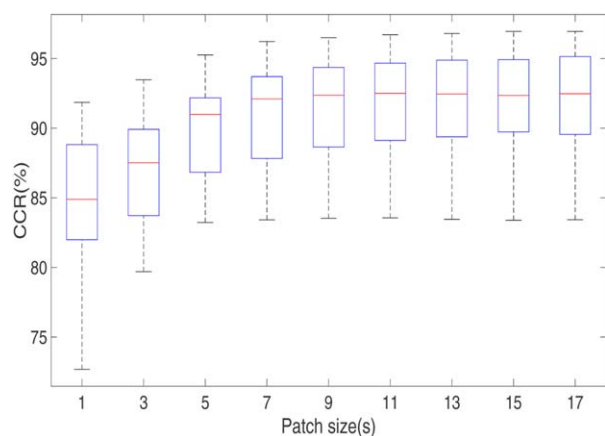


Figure 10. The box plots of M-FISH image classification accuracy using proposed method with different patch size. [Color figure can be viewed in the online issue, which is available at wileyonlinelibrary.com.]

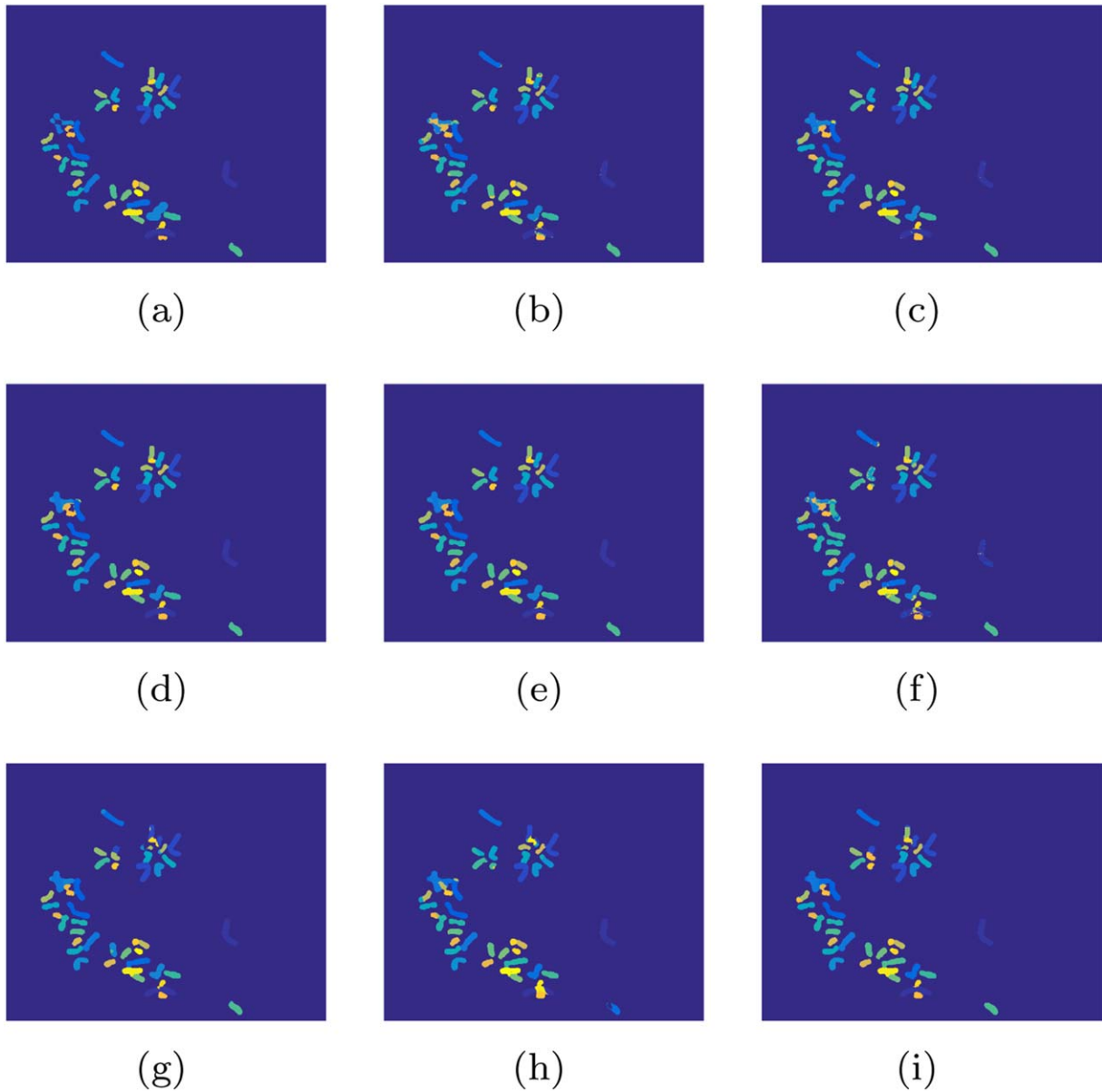


Figure 11. An example of the M-FISH image classification results by using different methods, where each class represented with a pseudo color. (a) Ground truth. (b) Proposed ($s=1$, CCR=88.56%). (c) Proposed ($s=5$, CCR=92.33%). (d) Proposed ($s=9$, CCR=93.04%). (e) Proposed ($s=13$, CCR=93.18%). (f) SparseRC (CCR=81.56%). (g) IAFCM (CCR=82.92%). (h) AFCM (CCR=72.14%). (i) FCM (CCR=78.61%). [Color figure can be viewed in the online issue, which is available at wileyonlinelibrary.com.]

Table 3. The computational time of the proposed method with different patch sizes

PATCH SIZE (S)	TRAINING	TEST
3	0:06:25	0:03:08
5	0:23:38	0:03:27
7	1:04:58	0:02:47
9	1:52:12	0:03:12
11	2:35:40	0:03:13
13	3:20:48	0:03:45
15	4:13:03	0:03:58
17	5:19:14	0:03:14

suppressed and thus the CCRs may increase. Figure 9 show the box plots of the results in Table 1. Five important statistics are given in the box plot: the sample minimum (smallest CCR), the lower quartile or first quartile, the median (middle value), the upper quartile or third quartile, and the maximum (largest CCR). From Figure 9, we can know that the CCRs of the proposed method and SparseRC method vary in a narrower range compared with other methods. This indicates both the proposed method and SparseRC method have a more stable performance. In addition, the proposed method has a higher CCR value with less variation than SparseRC.

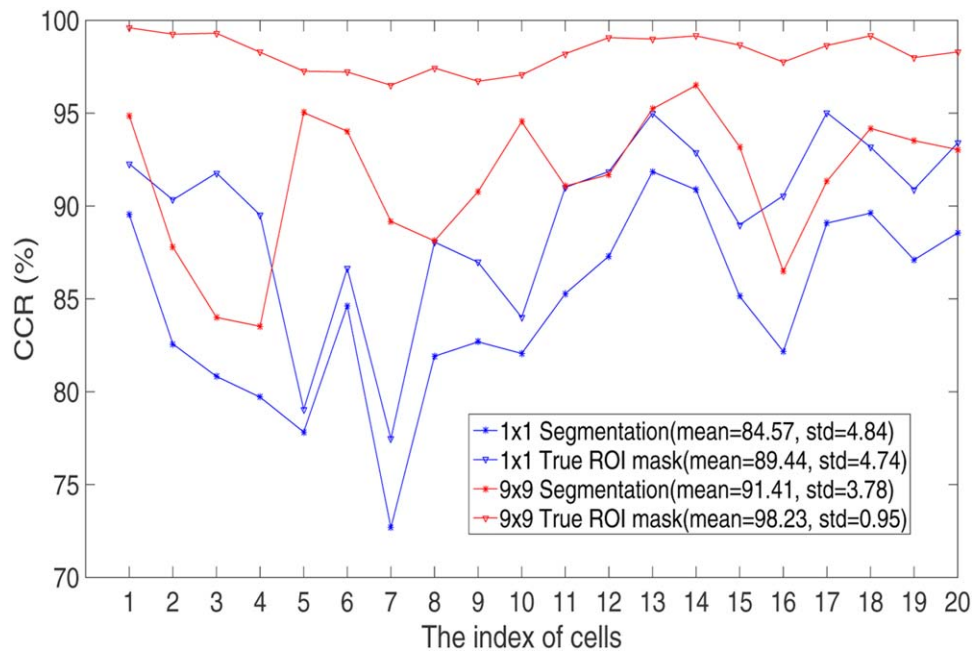


Figure 12. The CCRs with different ROI mask. [Color figure can be viewed in the online issue, which is available at wileyonlinelibrary.com.]

Table 2 shows the CCRs of the proposed method with different patch size. Figure 10 shows the box plots of results in Table 2. From Table 2, we can see that when $s < 9$, the CCRs increase along with increase of s , but when $s > 9$ the increase is not remarkable due to the loss of correlations between pixels with a large patch. Moreover, if the patch size is too large, the training vector will be very large too, which will increase both the computational time and storage space. We recommend the patch size to be 9×9 and the results are the best when compared with SparseRC, IAFCM, AFCM, and FCM methods in Table 1. We also know that the difference of the standard deviation between different patch size is not significant and $\max\{\text{std}\} < 5$, indicating that the proposed method with different patch sizes are all very robust and a moderate size of 9×9 is sufficient. Figure 11 shows an example of classification results of using different methods as well as the proposed method with four different patch size ($s=1, 5, 9, 13$). Each chromosome class is labeled and shown with a pseudo color. It can be seen that there are more isolated spots in the chromosomal regions of Figure 11f than those of Figure 11b. These isolated spots are mostly misclassifications, which can be reflected in the CCRs. The CCR of Figure 11f is 81.56%, which is lower than the CCR of Figure 11b 88.56%. As we can see from Figures 11c and 11d, when the patch size increases, the number of isolated spots become smaller and smaller. There almost have no isolated spots in Figure 11e, whose CCR is 93.18%. The CCRs in Figures 11g, 11h, and 11i are 82.92%, 72.14%, and 78.61%, respectively, which are not very high when compared with the proposed method.

Platform and Computational Time

All experiments were performed using MATLAB R2014b on a windows workstation with 6-core 2.40GHz CPUs(In-

tel(R) Xeon(R) CPU E5-2620 v3) and the memory(RAM) of 32.0GB. The MATLAB codes are available at <https://sites.google.com/site/minwang19891218/home/m-fish-image-classification>. To verify the practicability of the proposed method, we test on one cell to calculate the execution time. Table 3 shows the computational time of the proposed method with different patch sizes. From Table 3, we can see that the training time increases about 40 min along with the increase of patch size and the test time is relatively stable between 2 min and 4 min. As we have aforementioned, since the length of training vector is $5s^2$, a larger patch size will lead to a larger training vector, which will increase the computational load and storage memory. In the training phase, the parameter r and k (number of leading basis vectors) are set by a 10-fold cross validation, which will take a long time, especially when the length of training vector is large. The computation time of training phase in Table 3 is mostly used during cross validation. However, since training is usually performed off-line, computational time is not critical for the overall performance of the algorithm. Once we get the feature vectors of each chromosome class in the training phase, in test phase, we compute the low dimensional representation of each test pixel and get the class label by Eq. (6), which is very fast. According to the CCR values in Table 2 and the computation time in Table 3, the patch size of 9×9 is recommended.

DISCUSSIONS AND CONCLUSIONS

In summary, in this article, we proposed a patch-based tensor decomposition algorithm for M-FISH image classification by taking advantage of both spatial and spectral correlations of multi-channel images. To our knowledge, this is the first endeavor of applying tensor decompositions to

chromosome classification, which are able to incorporate multi-dimensional spectral information using tensors. There are three phases in the proposed method. First, a level set-based image segmentation method is used to segment the DAPI channel to get the mask of ROI, only within which the pixels are classified. Second, a training tensor is constructed for HOSVD, by which the features for each chromosome class are extracted simultaneously. Third, every pixel in the ROI mask is projected into a subspace to get the low dimensional representation. This feature subspace is shared by all the chromosome classes. We determine which class's feature vectors can best represent the projected pixel and assign the test pixel to this particular class. Results tested on the M-FISH database showed that the tensor decomposition-based algorithm (the patch size $s = 1$) can give better classification ratio than several existing methods including SparseRC, IAFCM, AFCM, and FCM. The use of patch (the patch size $s > 1$) can take advantage of the correlations between neighboring pixels and across different spectral channels, leading to better classification.

Although the proposed method gives the highest classification accuracy among the existing classifiers tested, there still have rooms for further improvement. The number of basis vectors for each chromosome class we use is the same, which is selected by a 10-fold cross validation. We can also use a different threshold value for the Σ_α in (3) to choose the number of basis vectors in B_α . In this way, the number of basis vectors we select in each chromosome class will be different and the methods in the feature selection will be more flexible, which may lead to a better classification. Figure 12 shows the results of proposed method with the true ROI mask and the segmented ROI mask. The patch sizes of 1×1 and 9×9 are used for the comparison. From Figure 12, we can see that the proposed method with patch size of 9×9 under the true ROI mask get the CCRs(%) with mean = 98.23 and std = 0.95, which is the best. As we aforementioned, the use of patch (the patch size $s > 1$) can take advantage of the correlations between neighboring pixels and across different spectral channels, which will suppress the noise effects. Under the same ROI mask, the differences of CCRs between different patch sizes are mainly due to the different levels of noise being suppressed. Analogously, under the same patch size, the differences of CCRs may also be due to the different ROI masks used. Since the ROI mask depends on the segmentation method, some other segmentation method using multichannel information such as proposed by Petros et al. (8) can be used to improve the classification results. Moreover, some preprocessing (e.g., color compensation, image denoising, and image enhancement) or postprocessing (e.g., smoothing the classification map) can be incorporated to further increase the accuracy of classification.

LITERATURE CITED

- Speicher MR, Ballard SG, Ward DC. Karyotyping human chromosomes by combinatorial multi-fluor fish. *Nat Genet* 1996;12:368–375.
- Schröck E, Manoir SD, Veldman T, Schoell B, Wienberg J, Ferguson-Smith MA, Ning Y, Ledbetter DH, Bar-Am I, Soenksen D, Garini Y, Ried T. Multicolor spectral karyotyping of human chromosomes. *Science* 1996;273:494–497.
- Liehr T, Claussen U. Multicolor-fish approaches for the characterization of human chromosomes in clinical genetics and tumor cytogenetics. *Current Genomics* 2002;3: 213–235.
- Choi H, Castleman KR, Bovik AC. Joint segmentation and classification of m-fish chromosome images. In: Proceedings of the Annual International Conference of the IEEE Engineering in Medicine and Biology, Vol. 26 III; 2004. pp 1636–1639.
- Sampat MP, Bovik AC, Aggarwal JK, Castleman KR. Supervised parametric and non-parametric classification of chromosome images. *Pattern Recognit*, 2005;38:1209–1223.
- Wang Y-P, Castleman KR. Normalization of multicolor fluorescence in situ hybridization (m-fish) images for improving color karyotyping. *Cytometry A* 2005;64:101–109.
- Schwartzkopf WC, Bovik AC, Evans BL. Maximum-likelihood techniques for joint segmentation-classification of multispectral chromosome images. *IEEE Trans Med Imaging* 2005;24:1593–1610.
- Karvelis PS, Tzallas AT, Fotiadis D, Georgiou I. A multichannel watershed-based segmentation method for multispectral chromosome classification. *IEEE Trans Med Imaging* 2008;27:697–708.
- Choi H, Castleman KR, Bovik AC. Color compensation of multicolor fish images. *IEEE Trans Med Imaging* 2009;28:129–136.
- Lee C, Gisselsson D, Jin C, Nordgren A, Ferguson DO, Blennow E, Fletcher JA, Morton CC. Limitations of chromosome classification by multicolor karyotyping. *Am J Hum Genet* 2001;68:1043–1047.
- Choi H-S, Castleman KR, Bovik AC. Segmentation and fuzzy-logic classification of m-fish chromosome images. In: 2006 IEEE International Conference on Image Processing; 2006. pp 69–72.
- Wang Y-P. Classification of m-fish images using fuzzy c-means clustering algorithm and normalization approaches. In: 2004. Conference Record of the Thirty-Eighth Asilomar Conference on Signals, Systems and Computers, Vol. 1; 2004. pp 41–44.
- Wang Y-P, Dandpat AK. Classification of multi-spectral fluorescence in situ hybridization images with fuzzy clustering and multiscale feature selection. In: 2006. GEN-SIPS'06. IEEE International Workshop on Genomic Signal Processing and Statistics; 2006. pp 95–96.
- Wang Y-P. Detection of chromosomal abnormalities with multi-color fluorescence in situ hybridization (m-fish) imaging and multi-spectral wavelet analysis. In: 2008. EMBS 2008. 30th Annual International Conference of the IEEE Engineering in Medicine and Biology Society; 2008. pp 1222–1225.
- Choi H, Bovik AC, Castleman KR. Feature normalization via expectation maximization and unsupervised nonparametric classification for m-fish chromosome images. *IEEE Trans Med Imaging* 2008;27:1107–1119.
- Eils R, Uhrig S, Saracoglu K, Sätzler K, Bolzer A, Petersen I, Chassery J-M, Ganser M, Speicher MR. An optimized, fully automated system for fast and accurate identification of chromosomal rearrangements by multiplex-fish (m-fish). *Cytogenet Genome Res* 1998;82:160–171.
- Saracoglu K, Brown J, Kearney L, Uhrig S, Azofeifa J, Fauth, C, Speicher MR, Eils R. New concepts to improve resolution and sensitivity of molecular cytogenetic diagnostics by multicolor fluorescence in situ hybridization. *Cytometry* 2001;44:7–15.
- Karvelis PS, Fotiadis D, Georgiou I, Syrrou M. A watershed based segmentation method for multispectral chromosome images classification. In: 2006. EMBS'06. 28th Annual International Conference of the IEEE Engineering in Medicine and Biology Society; 2006. pp 3009–3012.
- Karvelis PS, Fotiadis D, Tzallas A, Georgiou I. Region based segmentation and classification of multispectral chromosome images. In: CBMS'07; 2007. Twentieth IEEE International Symposium on Computer-Based Medical Systems. pp 251–256.
- Wang Y-P, Dandpat AK. A hybrid approach of using wavelets and fuzzy clustering for classifying multispectral fluorescence in situ hybridization images. *Int J Biomed Imaging* 2006(Article ID 54532):1–11.
- Sampat MP, Castleman KR, Bovik AC. Pixel-by-pixel classification of mfish images. In: 2002. Proceedings of the Second Joint 2002. 24th Annual Conference and the Annual Fall Meeting of the Biomedical Engineering Society EMBS/BMES Conference Engineering in Medicine and Biology, Vol. 2; 2002. pp 999–1000.
- Smilde A, Bro R, Geladi P. *Multi-Way Analysis: Applications in the Chemical Sciences*. Wiley; 2005.
- Ji T-Y, Huang T-Z, Zhao X-L, Ma T-H, Liu G. Tensor completion using total variation and low-rank matrix factorization. *Information Sci* 2016;326:243–257.
- Hackbusch W. *Tensor Spaces and Numerical Tensor Calculus*. Springer Science & Business Media, Vol. 42; 2012.
- Acar E, Yener B. Unsupervised multiway data analysis: A literature survey. *IEEE Trans Knowl Data Eng* 2009;21:6–20.
- Kolda TG, Bader BW. Tensor decompositions and applications. *SIAM Rev* 2009;51: 455–500.
- Khoromskij BN. Tensors-structured numerical methods in scientific computing: Survey on recent advances. *Chemometr Intell Lab Syst* 2012;110:1–19.
- Grasedyck L, Kressner D, Tobler C. A literature survey of low-rank tensor approximation techniques. *GAMM-Mitteilungen* 2013; 36: 53–78.
- Cichocki A, Mandic D, De Lathauwer L, Zhou G, Zhao Q, Caiafa C, Phan HA. Tensor decompositions for signal processing applications: From two-way to multiway component analysis. *IEEE Signal Process Mag* 2015;32:145–163.
- De Lathauwer L, De Moor B, Vandewalle J. A multilinear singular value decomposition. *SIAM J Matrix Anal Appl* 2000;21:1253–1278.
- Savas B, Eldén L. Handwritten digit classification using higher order singular value decomposition. *Pattern Recognit* 2007;40:993–1003.
- Lu H, Plataniotis KN, Venetsanopoulos AN. A survey of multilinear subspace learning for tensor data. *Pattern Recognit* 2011;44:1540–1551.
- Vasilescu MAO, Terzopoulos D. Multilinear analysis of image ensembles: Tensorfaces. In: *Computer Vision—ATECCV* 2002; 2002. pp 447–460.

34. Haardt M, Roemer F, Del Galdo G. Higher-order svd-based subspace estimation to improve the parameter estimation accuracy in multidimensional harmonic retrieval problems. *IEEE Trans Signal Process* 2008;56:3198–3213.
35. Phan AH, Cichocki A. Tensor decompositions for feature extraction and classification of high dimensional datasets. *IEICE Nonlinear Theory Appl* 2010;1:37–68.
36. Dunteman GH. *Principal Components Analysis*. Sage, No. 69; 1989.
37. Wold S. Pattern recognition by means of disjoint principal components models. *Pattern Recognit*, 1976;8:127–139.
38. Comon P, Jutten C. *Handbook of Blind Source Separation: Independent component analysis and applications*. Academic Press; 2010.
39. Cichocki A, Zdunek R, Phan AH, Amari S-I. *Nonnegative matrix and tensor factorizations: Applications to exploratory multi-way data analysis and blind source separation*. Wiley; 2009.
40. Bruckstein AM, Donoho DL, Elad M. From sparse solutions of systems of equations to sparse modeling of signals and images. *SIAM Rev* 2009;51:34–81.
41. Li C, Kao C-Y, Gore JC, Ding Z. Minimization of region-scalable fitting energy for image segmentation. *IEEE Trans Image Process* 2008;17:1940–1949.
42. Cao H, Deng H-W, Li M, Wang Y-P. Classification of multicolor fluorescence in situ hybridization (m-fish) images with sparse representation. *IEEE Trans NanoBiosci* 2012;11:111–118.
43. Cao H, Deng H-W, Wang Y-P. Segmentation of m-fish images for improved classification of chromosomes with an adaptive fuzzy c-means clustering algorithm. *IEEE Trans Fuzzy Syst* 2012;20:1–8.
44. Pham DL, Prince JL. An adaptive fuzzy c-means algorithm for image segmentation in the presence of intensity inhomogeneities. *Pattern Recognit Lett* 1999; 20:57–68.